JOURNAL OF MATERIALS SCIENCE 30 (1995) 1863–1871

Mechanical properties in the initial stage of sintering

P. ARATÓ, E. BESENYEI, A. KELE, F. WÉBER
Research Institute for Technical Physics, Budapest, P.O. Box 76, H-1325, Hungary

Silicon nitride-based ceramics with different compositions were sintered in the 60%–90% range of theoretical density. Linear correlations between the apparent density and the modulus of elasticity, the three- and four-point bend strengths or the Vickers hardness, were observed. The slopes of the straight lines were nearly the same for all compositions. Furthermore, the modulus of elasticity, hardness, fracture toughness and strength were calculated as functions of density by modelling the structure as a random arrangement of spheres as suggested by Fischmeister and Arzt. The relationships obtained have been compared with the measured ones.

Nomenclature

a	average contact area
a_c	increase of the area of a crack
A	area of the reference plane
b	size of the critical defect
c	constant in Equation 4
D	density
D_0	density before shrinkage
D_T	theoretical density
$\boldsymbol{e}$	direction of macroscopic strain
E	modulus of elasticity
E_0	modulus of elasticity of the dense material
f	force loading a contact
$f(\theta)$	projection of force f to $\boldsymbol{e}$
F	force loading the reference plane
g	geometry parameter in the Griffiths relationship
H	hardness
K_{IC}	fracture toughness
N	number of particles in unit volume
$N(\theta)$	the fraction of N in a given spherical angle
$n(\theta)$	number of particles in the volume around the reference plane
P	porosity
R	initial particle radius
R'	particle radius after fictitious growth
R''	particle radius after redistribution of material
R_{SQ}	shared correlation coefficient
S	surface energy of the defect
$\boldsymbol{v}$	vector connecting the centres of neighbouring particles
W	work necessary for increase the area of a crack
Z	average coordination number
Z_0	initial coordination number
ε	strain
ε_T	strain at theoretical strength
σ	strength
σ_T	theoretical strength (limit of elasticity)
θ	angle between $\boldsymbol{v}$ and $\boldsymbol{e}$

1. Introduction

The sintering process can be divided into three stages: initial, intermediate and final [1, 2]. In the initial stage, necks develop between the grains, and this stage ends when the necks begin to impinge. The intermediate stage can be characterized by networks of interconnected grains and interconnected open pores, while in the final stage the pores become isolated. Some authors [3, 4] do not distinguish between the second and third stages; on the other hand the rearrangement of particles before they begin to coalesce may be considered as a separate stage [3, 5]. A large number of papers has been published modelling the different stages, predicting the morphology of the structure and the kinetics of the densification. Different stackings of spheres were suggested to describe the initial or the initial and intermediate stages [3, 6–8], while the intermediate stage could be modelled by a cellular array of cylinders [9].

Silicon nitride-based ceramics developed for structural applications are usually completely densified. There are numerous studies concerning the relationships between their mechanical properties and chemical composition, phase composition or different processing parameters (e.g. [5, 9–13]). The density of samples was frequently in the range 3–3.3 $g\,cm^{-3}$ (0.9–1 theoretical density, TD), relatively few data are available for lower densities. Yeheskel and Gefen [14] measured the modulus of elasticity for silicon nitride-based materials of TD 0.55–0.95 prepared by different procedures; Godfrey [15] determined the flexural strength of pressureless sintered ceramics containing different additives having 0.85–1 TD, while Heinrich *et al.* [16] measured the same quantity for reaction-sintered silicon nitride samples with TD 0.45–1. The fracture toughness as well as the modulus of elasticity and the flexural strength of reaction-sintered Si_3N_4 were measured by Rice *et al.* [17] for TD 0.4–0.8. Datta *et al.* [18] carried out a regression analysis for the modulus of elasticity–porosity relationship using

0022–2461

different approximative functions. A total of 156 data were collected in the TD 0.62–1 range.

A systematic study of the development of microstructure and the variation of mechanical properties during the initial stage of sintering was carried out by Coronel *et al.* [4] on commercial glass powder. The value of the volume fraction after sintering ranged between 0.63 and 0.98; they presumed the microstructure to be an evolution from a stacking of spheres to a body containing isolated pores. The transition between the two types was observed at ~ 0.75 TD. This type of experiment on silicon nitride-based ceramic is not known to the authors.

The understanding of the relationship between the structure and mechanical properties of a porous body is a different task. It is clear that the morphology of the structure must be taken into account. The question is, to what extent are the average structural features, such as grain size and porosity, characteristic and where should the weakest-link statistics be applied [19]? The published calculations based on models of microstructures concentrated on a single property, either on the pressure required for isostatic pressing [3, 20, 21], or on the modulus of elasticity [22].

The Griffiths relationship is often used to connect the strength, σ, with structural parameters

$$\sigma = gK_{IC}(b)^{-1/2} \quad (1)$$

where b is the half-size of the critical defect, g is a geometry parameter (0.774 for a small, flat semicircular, surface flaw with radius, b), K_{IC} is the fracture toughness given by

$$K_{IC} = (2SE)^{1/2} \quad (2)$$

where E is the modulus of elasticity and S is the surface energy of the defect. The difficulty in applying the Griffiths equation is in the shortage of knowledge on the defects controlling the fracture.

Our aim was to examine experimentally and theoretically the mechanical properties of partially sintered silicon nitride-based ceramics in the 0.6–0.9 TD range. It is thought that the investigation of this stage may be interesting not only in theory but also in practice, because the properties of a fully densified ceramic depend on the way in which the sintering was conducted.

2. Experimental procedure

2.1. Materials

Mixtures of Si_3N_4, AlN, Al_2O_3 and Y_2O_3 powders were milled in ethanol in a planetary-type alumina ball mill. The composition of materials is given in Table 1 and Fig. 1; the equivalent oxygen content was calculated without taking yttria into account. The selected series is suitable to detect the effect of silicon nitride content. Samples were compacted by dry pressing at 290 MPa. The sintering experiments were carried out in an ABRA-made HIP apparatus in 1–2 MPa high-purity nitrogen using BN embedding powder. The heating rate was 25 °C min^{-1}. After reaching a certain temperature, T (1230–1730 °C), the sintering cycle was interrupted and the samples were cooled at 40 °C min^{-1}.

TABLE I Composition of materials (mass %)

	Si_3N_4	AlN	Al_2O_3	Y_2O_3
A	90	0	4	6
B	87	4	4	5
C	84	8	4	4
D	76.9	15	4.1	4
E	69	21	6	4

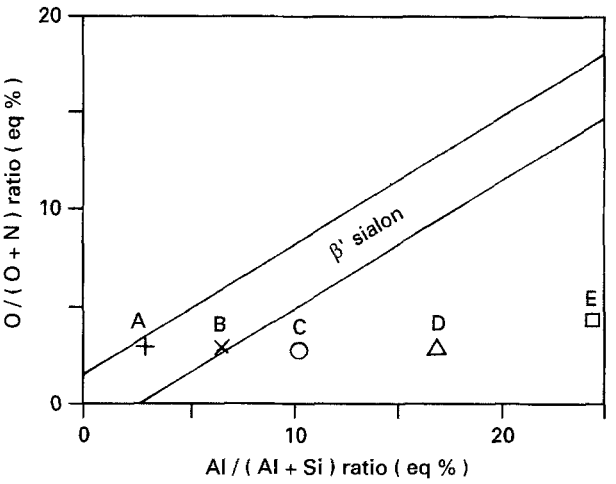

Figure 1 Composition of materials.

2.2. Methods

Samples were characterized by the apparent and bulk densities, which were measured using the water immersion method after 72 h impregnation. The apparent density was also calculated from the geometrical and weight data; the results obtained coincided, within experimental error, with those obtained by the Archimedes method. The modulus of elasticity and the four-point bend strength were determined at room temperature with spans of 40 and 20 mm. The three-point strength was measured on the same samples (span 20 mm). Hardness was determined by a Vickers diamond indentor on a polished surface; the load was 5 N. Fracture toughness, K_{IC}, was calculated from the length of the indent cracks using Niihara's formula for short cracks. The microstructure analysis was carried out by scanning electron microscopy on polished samples etched in NaOH. The ratio of α and β phases was determined using Gazzara and Messier's method [23].

3. Results

3.1. Densification

The apparent density is shown in Fig. 2 as a function of the highest temperature of heat treatment, T. Slight differences were observed between the rates of densification: B was the most active material. The density began to increase with increasing temperature only if the value of T exceeded 1400 °C. Its value, averaged for the first four heat treatments, was only slightly

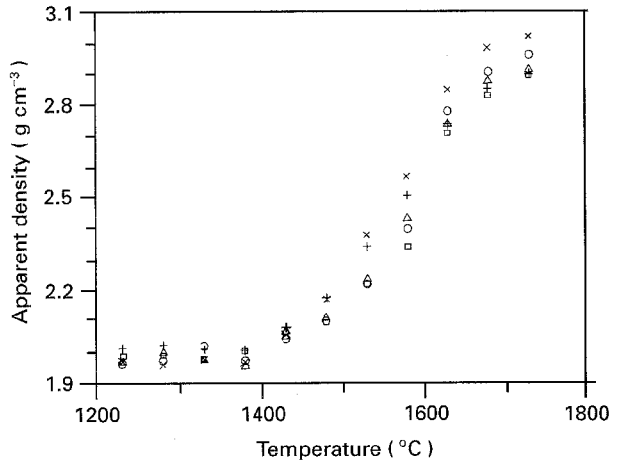

Figure 2 Apparent density as a function of the highest temperature of heat treatment. Compositions: (+) A, (×) B, (○) C, (△) D, (□) E, (see Fig. 1 and Table I).

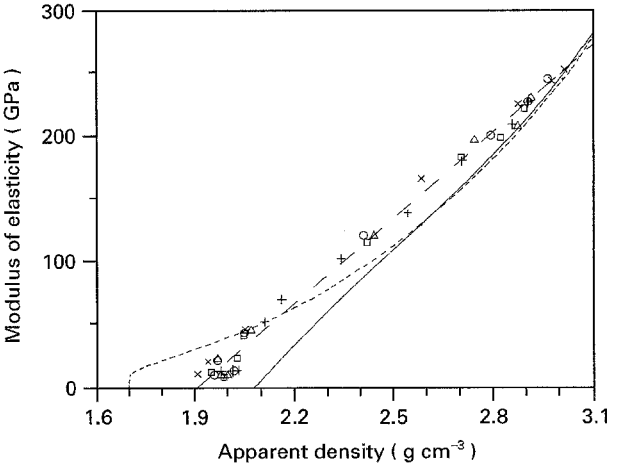

Figure 4 Modulus of elasticity as a function of the apparent density. Compositions as for Fig. 2. (———) Best fit straight line, (——) Equation 14, (- - -) Wang's calculation.

TABLE II Characteristic densities of materials

Material	Density (g cm^{-3})		
	Highest	Compacted	Initial
A	3.25	1.99	2.01
B	3.25	1.95	1.97
C	3.22	1.95	1.98
D	3.25	1.98	1.98
E	3.27	1.98	1.99

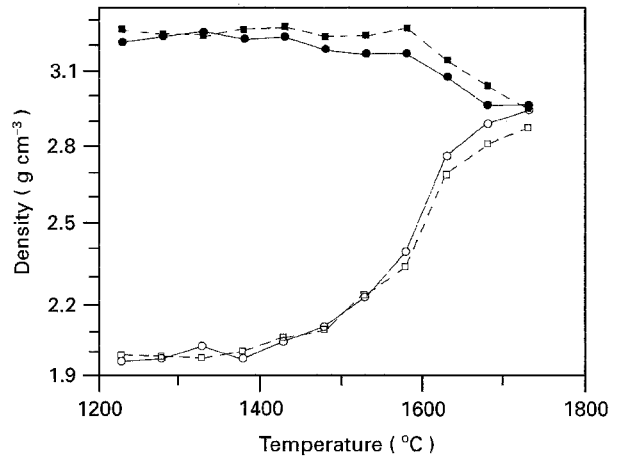

Figure 3 (○, □) Apparent and (●, ■) bulk densities for materials (○, ●) C and (□, ■) E as a function of the highest temperature of heat treatment.

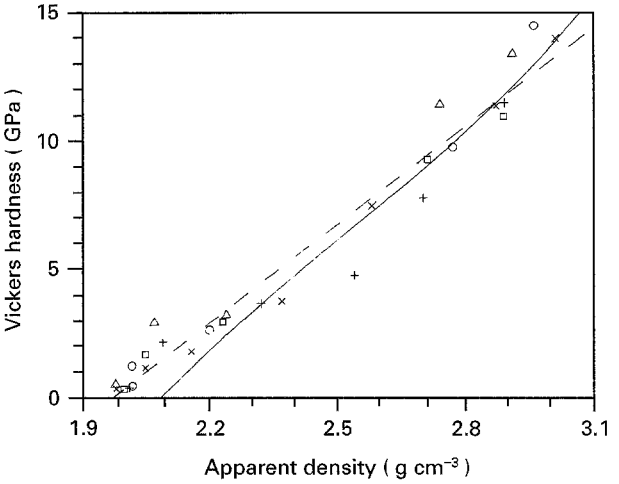

Figure 5 Vickers hardness as a function of the apparent density. (———) Best fit straight line, (——) Equation 15 for $\sigma_T = 6.1$ GPa theoretical strength.

higher than the density after compaction (compare the initial and compacted densities in Table II).

The density of the pore closure can be determined [24] by plotting the apparent and bulk densities as a function of temperature (see Fig. 3). The first closed pores appear when the bulk density begins to decrease, while the closure of the open channels is reflected by the equality of the apparent density and bulk density. The value of apparent density, at which the bulk density begins to decrease, is in the 2.4–2.6 g cm^{-3} range for all materials. The matching of the two curves was achieved at 1730 °C for materials C (Fig. 3, full lines) and B; the obtained densities of pore closure were 2.96 and 2.98 g cm^{-3}, respectively. In the case of materials A, D and E (Fig. 3, dotted lines) a small difference between the apparent and bulk densities occurred even at the highest temperature, but the range 2.89–2.97 g cm^{-3} probably contained the matching value.

Numerous samples from the materials examined were heat treated using pressureless or high-pressure processes [24–26]. The values of the highest possible densities were determined by measuring the densities of these samples; they were taken as the theoretical densities (see first column of Table II). The calculation of TD from structural data was not possible owing to the lack of sufficient information about the intergranular phase. For all materials, the measured compaction density was equivalent to 0.61 TD; at 0.74–0.80 TD the development of the closed pores began; the density of pore closure was 0.90–0.92 TD.

3.2. Mechanical properties

The modulus of elasticity as well as the hardness and bend strength increased with increasing apparent

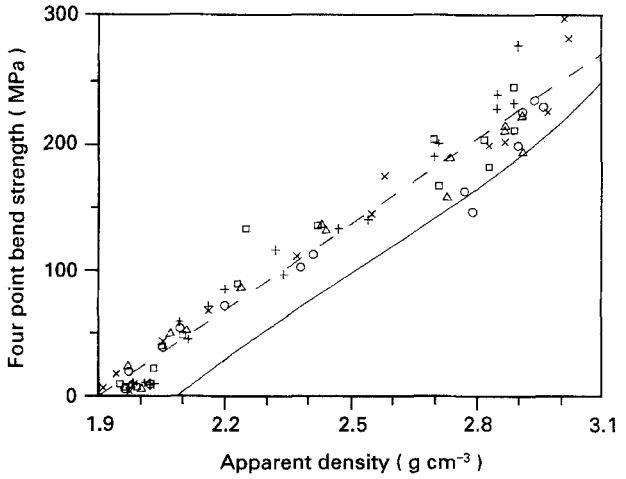

Figure 6 Four-point bend strength as a function of the apparent density. (— — —) Best fit straight line, (——) Equation 21 for 80 μm defect size.

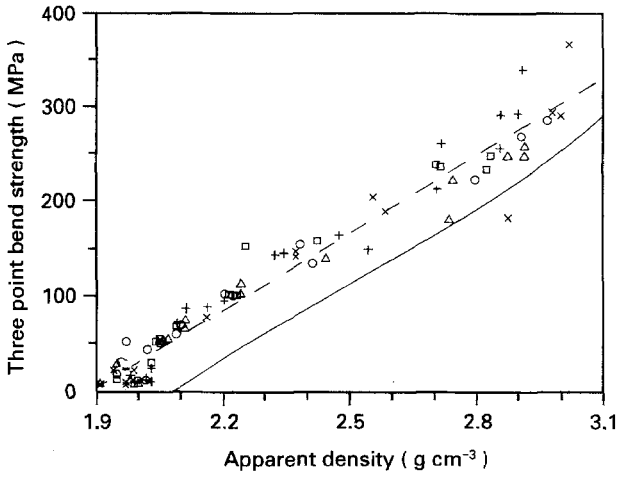

Figure 7 Three-point bend strength as a function of the apparent density. (— — —) Best fit straight line, (——) Equation 21 for 55 μm defect size.

density as expected. It was striking, however, that at a given density the values obtained for different materials were very similar (see Figs 4–7). The modulus of elasticity was certainly a linear function of density (Fig. 4); in the case of other properties, the scatter of points around the straight lines of best fit was greater (Figs 5–7), but the trend seemed to be obvious.

To obtain a more exact evaluation of the results, a linear regression was performed. The first and second material groups of Table III gives the slopes of property–density lines and the intersections of these lines with the horizontal axes for the different materials. The results of analysis of complete data set are given in the third group. The densities belonging to the intersections of these lines with the horizontal axes are also shown. The results of analysis of the total data set measured on samples with different compositions can be seen.

The measured moduli of elasticity fitted well with the common straight line (R_{SQ}, the shared correlation coefficient, was 0.99), the differences between the values of slopes or intersections of lines belonging to different materials were smaller than their standard deviations, S.D. (6–8 GPa cm^3 g^{-1}). The density value of the crossing of a common line with the $E = 0$ axis (1.91 g cm^{-3}), was slightly smaller than the compacted density.

The scattering of the hardness values around the common straight line was wider than that of the moduli, the S.D. of the individual slopes was 1.4–0.5 GPa cm^3 g^{-1} (the number of measurements was too small), therefore the significance of the differences between them is low. The density at zero hardness coincided with the compaction density within the S.D.

The differences between the slopes of strength–density curves of different materials both for four- and three-point measurements exceeded the S.D.S (typically 10–15 MPa cm^3 g^{-1}). The strength of material A was higher, and that of materials C and D was lower, than the average. The density of zero strength was smaller by 1 S.D., than the compaction density.

The accuracy of our toughness measurements was not sufficient to determine the density dependence. $K_{IC} = 3.8$ MPa m$^{1/2}$ was a typical value in the 2.5–3.0 g cm^{-3} (TD = 0.75–0.9) range.

The amount of α phase was 0.85 ± 0.1 for all samples except three; for them it was 0.68, 0.57, 0.56. It is not possible to deduce anything about the effect of phase composition on the mechanical properties from the examined set of samples. The results of regression analysis did not change significantly after erasing the data of these three samples.

4. Model of the structure

Three experimental facts had to be taken into account when choosing a model for further considerations. (1) The mechanical properties were linear functions of density in the 0.6–0.9 TD range. (2) The parameters of these lines only slightly depended on the composition. (3) All the properties has zero value at 0.58–0.61 TD. Fact 1 suggests that there is no substantial change in the mechanism of densification in the 0.6–0.9 TD range. Fact 3 contradicts a model supposing an array of cylinders. The observed structure (Fig. 8) looks like an arrangement of spheres. Fischmeister and Arzt [3] developed a model (FA model) for describing the densification of an irregular packing of spherical particles. If the mechanical properties of a porous material are controlled by the number and size of interparticle contacts, this realistic concept may be the competent basis for their calculation.

In the FA model, the spheres have equal radii, R, and their packing is initially dense and random. The densification treatment is carried out by replacing the decrease in the centre-to-centre distance of the spheres by a fictitious increase of their radii from R to R' (Fig. 9a, b). The two situations are geometrically equivalent; the scale factor is R'/R. R' is related to the density D by

$$R'/R = (D/D_0)^{1/3} \quad (3)$$

where D_0 is the relative density before shrinkage; for dense random packing $D_0 = 0.64\, D_T$ where D_T is the theoretical density.

In the FA model the average coordination number, Z, is a linear function of R'

$$Z = Z_0 + c(R'/R - 1) \quad (4)$$

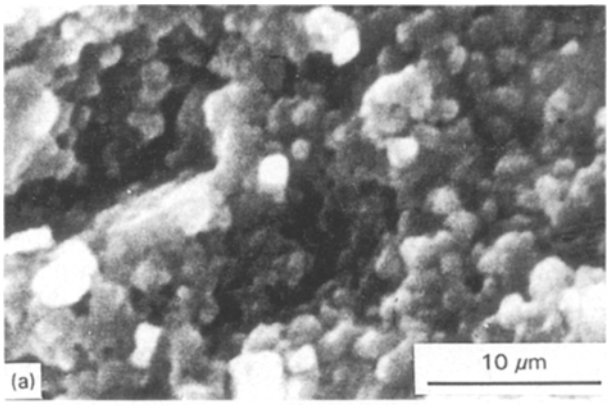

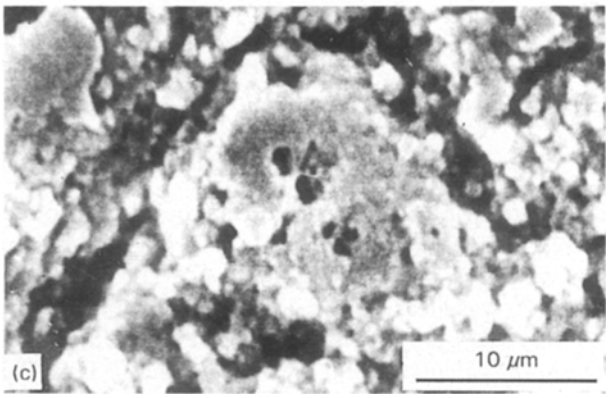

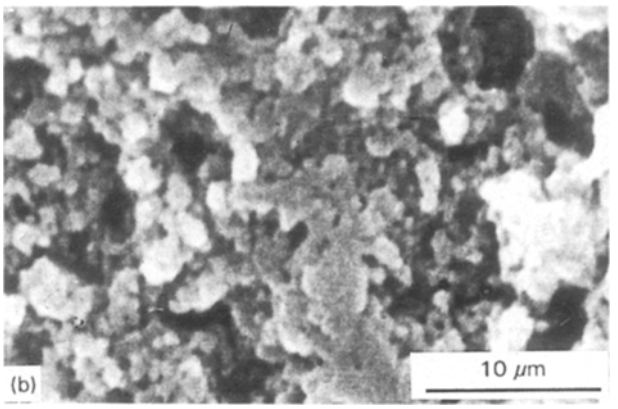

Figure 8 Microstructure of material C heat treated to (a) $T = 1230\,°C$, (b) $T = 1580\,°C$, (c) $T = 1680\,°C$.

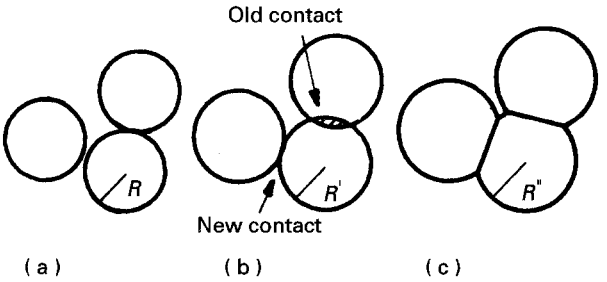

Figure 9 FA model: (a) initial state, (b) after a fictitious grain growth, (c) after the redistribution of material.

where $Z_0 = 7.3$ is the initial coordination number, while the second term refers to the new contacts developing during densification; $c = 15.5$. As a result of the size change, the initially contacting spheres would overlap, and the material is squeezed out from the contact zone (darkened area in Fig. 9b). It was assumed that the excess material was distributed evenly over those parts of the sphere surfaces that were not taken up by the old and new contacts (Fig. 9c). The redistribution process resulted in a further increase of the radius to R''

$$R'' = R' + \frac{4Z_0(R' - R)^2(2R' + R) + c(R' - R)^3(3R'/R + 1)}{12R'[4R' - 2Z_0(R' - R) - cR(R'/R - 1)^2]} \quad (5)$$

In the calculation of Equation 5, the increase of coordination number and the decrease of free surface due to redistribution, were neglected. The average contact area, a, in the same approximation was

$$a/R^2 = \pi[3(R''^2 - R^2)Z_0 + cR^2 + cR''^2(2R''/R - 3)]/3ZR'^2 \quad (6)$$

The FA model was found to be valid up to 0.9 TD, when it was applied to the compaction of spherical bronze powders [3]. At this density level the impingement of adjacent contacts began. The resemblance between the model and the real structure of silicon nitride-based ceramics is weaker than in the case of bronze powder. Our materials contained, in addition to Si_3N_4 grains, large grains of other components (Fig. 8a) in the beginning, and a certain amount of intergranular phase later. The application of the FA model to silicon nitride ceramic may be arbitrary; its outcome, however, is in surprisingly good accordance with the observations:

(1) no change is predicted in the mechanism between the start of densification and 0.9 TD; (2) the model is purely geometrical, and the composition of spheres plays no role in it. We note that the composition of the material affects the amount and viscosity of the liquid phase [5, 13] resulting in differences between kinetics, but this effect may be neglected when mechanical properties belonging to the same *density* are compared; (3) the theoretical initial density, 0.64 TD, is only slightly higher than the measured one, 0.61 TD. Wang [22] calculated the modulus of elasticity of porous materials supposing a simple cubic array; in this case the value of D_0 is 0.52 TD. The results of our density measurements seemed to be contrary to the FA model, because the formation of closed pores started at 0.74–0.80 TD and finished at 0.90–0.92 TD. It is believed, however, that in the 0.74–0.90 TD range, the network of soft intergranular phase closed the pores, not the firm intergranular contacts.

5. Calculation of mechanical properties

5.1. Modulus of elasticity

There are two well-known approximations for calculating the elastic properties of a polycrystalline body; in the Reuss model each grain feels the same stress, while in the Voigt model the strain is homogeneous.

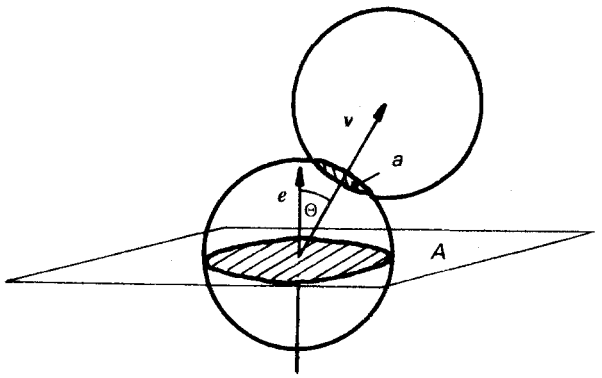

Figure 10 Geometry used in the calculation of modulus of elasticity. A is the reference plane, $\boldsymbol{e}$ its normal vector shows the direction of the macroscopic strain, vector $\boldsymbol{v}$ connects the centres of two neighbouring spheres, a is the contact area.

We computed the force loading a reference plane perpendicular to the direction of strain, applying the Voigt approximation. The real stress field was replaced by forces connecting the centres of contacting spheres. If a vector, $\boldsymbol{v}$, connecting the centres of neighbouring particles, is parallel to the direction of the macroscopic strain, $\boldsymbol{e}$, force, f, acting in the given contact is

$$f = E_0 a\varepsilon \tag{7}$$

where E_0 is the modulus of elasticity of the dense material (it differs from the effective modulus of the porous body, E), a is the contact area, ε is the strain.

Let the angle between $\boldsymbol{v}$ and $\boldsymbol{e}$ be θ (Fig. 10), then it can be assumed that the projection of force to $\boldsymbol{e}$ is

$$f(\theta) = f\cos\theta \tag{8}$$

Vector $\boldsymbol{v}$ cuts the reference plane if the distance of the centre of the "upper" sphere and the plane is smaller than $2R\cos\theta$ that is this centre is inside a volume $2AR\cos\theta$, where A is the area of the plane. The number of contacts in unit volume is $NZ/2$, where N is the number of particles in a unit volume. N is related to the density by

$$4\pi R^3 N/3 = D/D_T \tag{9}$$

The number of contacts for which the angle of $\boldsymbol{v}$ and $\boldsymbol{e}$ is between θ and $\theta + d\theta$ in unit volume $N(\theta)$ is

$$N(\theta) = NZ\sin\theta/2\, d\theta \tag{10}$$

The number of such contacts in volume $2AR\cos\theta$ is

$$n(\theta) = 2ARn(\theta)\cos\theta \tag{11}$$

The force, F, loading the reference plane can be obtained by using Equations 8, 10 and 11 and by integrating for θ

$$F = \int_0^{\pi/2} fNARZ\cos^2\theta\sin\theta\, d\theta \tag{12}$$

The definition of E is

$$F = AE\varepsilon \tag{13}$$

From Equations 7, 9, 12 and 13

$$E = E_0(D/D_T)Za/4R^2\pi \tag{14}$$

The value of E computed from Equation 14 is plotted in Fig. 4 as a function of density. The FA model gave the values of Z (Equation 4) and a/R^2 (Equation 6); 330 GPa was measured on dense α sialons for E_0 [26], D_T was 3.25 g cm^{-3} (Section 3.1). The agreement between the calculated and measured values is fair. The only significant difference is that the density belonging to zero modulus is smaller than $D_0 = 0.64$ predicted by the FA model, this deviation may be attributed to the fact that in our experiments the particles of starting powder were not spheres with equal radii.

Fig. 4 also shows the density dependence of the modulus of elasticity according to Wang's prediction (the curve was calculated from data of Table III of [22], with $E_0 = 330$ GPa, $D_T = 3.25$ g cm^{-3}). There were significant differences between his derivation and ours. He supposed that the centres of spheres formed a primitive cubic lattice consequently Z is a constant number (6), while in the FA model the array was random and Z increased. Furthermore, Wang exactly computed the force loading a contact in the ideal case, then corrected the result for the misalignment of the

TABLE III Results of linear regression. The slopes and their standard deviations (S.D.) are given in GPa cm^3 g^{-1}, GPa cm^3 g^{-1}, MPa cm^3 g^{-1}, MPa cm^3 g^{-1}, respectively, the intersections and their S.D.s are given in g cm^{-3}

Material		Young modulus	Vickers hardness	Four-point strength	Three-point strength
A	Slope	234	11.2	261	318
B	Slope	228	13.2	233	276
C	Slope	233	13.7	205	260
D	Slope	231	13.7	211	250
E	Slope	228	11.8	221	281
A	Intersection	1.93	1.97	1.95	1.94
B	Intersection	1.88	2.00	1.90	1.88
C	Intersection	1.91	1.98	1.89	1.86
D	Intersection	1.91	1.92	1.88	1.87
E	Intersection	1.91	1.95	1.88	1.88
All	slope	231	12.8	226	278
All	intersection	1.91	1.97	1.90	1.89
All	R_{SQ}	0.99	0.97	0.96	0.95
All	S.D. (slope)	3	0.5	5	6
All	S.D. (intersec.)	0.04	0.11	0.10	0.09

array and for the "hinging" effect of necks. Simplifying assumptions were used for estimating the porosity dependence of corrections. We described the angle dependence of the contact force by Equation 8, which is wholly hypothetical. In spite of dissimilarity of postulations, the calculated curves practically coincide in the 0.7–0.9 TD range, while its deviation is obvious at low values where the difference between the models in initial density is effective.

5.2. Hardness

In the case of hardness measurements, the stress field around the indentor destroys the intergranular contacts. Supposing that the material is an ideal elastic–brittle type, a contact is broken if its deformation exceeds the limit of elasticity. The penetration of the indentor stops when the stress in intergranular contacts becomes lower than the theoretical strength, σ_T. As the value of the equivalent uniaxial stress in the plane of the indentor equals one-third of the hardness, H, from Equations 7 and 13, we obtain

$$H = 3E/E_0\sigma_T \quad (15)$$

that is, the hardness is proportional to the effective modulus of elasticity. The measurements really showed that both properties were linear functions of the density. Neglecting the small difference between the intersections, we find from the slopes of Table III, that $H/E = 0.055$ and $\sigma_T = 6.1$ GPa. The curve calculated using this value is given in Fig. 5. Note that Equation 15 is generally valid, while Equation 14 is valid only in the initial stage of sintering.

5.3. Toughness

The value of toughness depends on the energy needed for creating a new surface. When the thickness of a crack is smaller than the particle size, its area can increase if the contacts in its plane have been broken. The deformation necessary to achieve the fracture of a contact, ε_T, is

$$\varepsilon_T = \sigma_T/E_0 \quad (16)$$

When the area of the crack increases by a_c, the volume of the deformed zone is $2a_cR$; consequently the deformation work, W, is

$$W = \sigma_T^2 a_c R E/E_0^2 \quad (17)$$

The surface energy equals

$$S = W/2a_c \quad (18)$$

Using Equations 2, 16 and 18

$$K_{IC} = \sigma_T R^{1/2} E/E_0 \quad (19)$$

The value of K_{IC} can be calculated from Equations 14 and 19, the results are given in Fig. 11. The $2R$ particle size is 0.6 μm for the LC12 Si_3N_4 powder used. The obtained value is 1.0 MPa $m^{1/2}$ for 0.75 TD, and 2.3 MPa $m^{1/2}$ for 0.9 TD.

The increase in toughness suggested by Equation 19 has not been detected by our measurements. The measured length of the indentation cracks was about 2–8 μm, therefore their relative error was high. The experimental value of toughness, 3.8 MPa $m^{1/2}$ was larger than the calculated one.

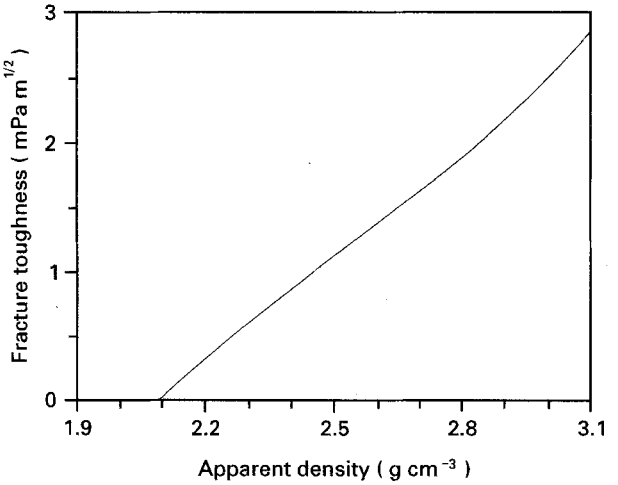

Figure 11 Fracture toughness as a function of the apparent density. (——) Equation 19 for $\sigma_T = 6.1$ GPa theoretical strength and $R = 0.3$ μm initial particle radius.

The calculation presented is not valid, if large elongated grains "bridge the crack" [12, 27] and hinder its extension.

5.4. Strength

In the preceding sections the deformations of particular contacts were taken as separate processes. This assumption may be reasonable in the range of elastic deformation or in the case of indentor loading, but is surely unrealistic when the bend strength is determined. If the failure occurred when the average stress in the contacts reached σ_T, the strength would be according to Equations 13 and 16

$$\sigma = E/E_0\sigma_T \quad (20)$$

The measured strength was lower by one order of magnitude than the value given by Equation 20 (e.g. at 0.75 TD it was 120–160 MPa and 1.2 GPa, respectively).

In fact, in a bending experiment the extension of a single defect results in the failure of the sample. Such a defect may be, for instance, the lack of a group of grains or the relative weakness of contacts at some places due to the local shortage of liquid phase necessary. From Equations 1 and 19

$$\sigma = \sigma_T R^{1/2} E/E_0 g(b)^{-1/2} \quad (21)$$

If the defect size, b, does not change during the coalescence of particles, the strength is proportional to the effective modulus of elasticity, and consequently to the density. This linear relationship was observed in our experiments. The differences between the slopes of the strength–density curves of different materials (first rows of Table III) indicate that the defect size depends on the composition. Using Equation 21 and taking 0.774 for g we obtained 65–100 μm as the defect size for four-point bending and 40–70 μm for three-point bending. In Figs 6 and 7 the strength–density curves calculated for 80 and 55 μm, respectively, are shown.

The difference between the four- and three-point slopes reflects that the volume of the deformed zone affects the size of the critical defect. This effect can be analysed by using statistical methods.

It must be emphasized that Equation 21 is valid only if the particles are spheres, they are connected by isolated contacts, and the characteristic defect size does not change during sintering. Different methods are used to produce a microstructure *not* fulfilling these conditions but giving a high strength [19, 27]. The success of these attempts, however, may depend on some features of the structure development during the early stages of sintering.

6. Comparison with published measurements

So far the calculated values of mechanical properties have been compared with our own measurements. By comparing them with the results of other studies it is possible to test the range of validity of the calculation. To do this it is suitable to convert the slopes of property–density lines (Table III) to slopes of property–relative density lines. The result for modulus of elasticity is 751 GPa, for hardness 41.5 GPa, for the four- and three-point strengths 734 MPa and 903 MPa, respectively.

Yeheskel and Gefen [14] measured the relationship between the modulus of elasticity and density. For five samples with 65 ± 22% α content, they obtained

$$E = 337(1 - 2.23P) = 337 - 752P \quad (22)$$

where P was the porosity

$$P = 1 - D/D_T \quad (23)$$

The porosity of these samples was between 0.28 and 0.46. The measured slope (752 GPa) was equal to our result (751 GPa), while the intersection (0.55 TD) was slightly smaller. Values of 200 GPa $cm^3 g^{-1}$ (638 GPa) can be calculated for the slope and 1.87 g cm^{-3} (0.59 TD) for the intersection from measurements by the same authors on another set of samples ([10] Fig. 8).

An exponential density function was suggested by Rice *et al.* [17]

$$E = 345\exp(-3.7P) \quad (24)$$

Approximating linearly this function in the $P = 0.1$–0.4 range, 533 GPa was obtained for the slope; this value is smaller than ours. Their samples were manufactured by reaction sintering, and the modulus was 50 GPa at $P = 0.5$, suggesting that the number of contacts differs from that supposed by the FA model.

Datta *et al.* [18] proved that in the case of high porosity a linear elasticity–porosity function gave almost as good fit with the measured data as exponential formulae. The slope calculated for the $P = 0.10$–0.38 range was 524 GPa.

The modulus of elasticity and the hardness were measured simultaneously in certain papers [10, 11]. The value of theoretical strength can be calculated from their ratio (Equation 15). We obtained 5.5–6 GPa for three pressureless sintered samples [11], 4.5–5.5 GPa for four HIPed samples [10], and 3 GPa for a single sample [10].

The variation of toughness in the function of the porosity was measured by Rice *et al.* [17]

$$K_{IC} = 3.5\exp(-2.4P) \quad (25)$$

Equation 25 gives 2.8 MPa $m^{1/2}$ for 0.1 porosity; this value is not far from the results of our calculations (Equation 19), but the decrease with increasing porosity is significantly smaller than our prediction.

The density dependence of the four-point strength of reaction-bonded silicon nitride was found to be exponential [16, 17]. A linear approximation in the 0.1–0.4 porosity range gave 613 MPa for the data of Heinrich *et al.* [16], and 646 MPa for results of Rice *et al.* [17].

Godfrey [15] supposed a linear relationship between the density and the strength of pressureless sintered disc samples; the slope was 580 and 790 MPa $cm^3 g^{-1}$ for two different starting powders. The covered density range was 2.8–3.4 g cm^{-3}, the scatter of points was significant ($R_{SQ} = 0.28$ or 0.85).

Hayashi and Kosakai measured the three-point strength and the hardness of pressureless sintered material [28]. According to Equations 15 and 21, their ratio is proportional to $(b/R)^{1/2}$. Six of the samples had a relative density in the 0.86–0.96 TD range, the ratio of the hardness and the strength was 20.2–20.5 for three samples containing a certain amount of additive and 22.5–22.9 for the other three with other compositions, suggesting that the critical defect size did not change in this density range.

The outlined analysis of published results showed that proportionalities could often be observed between the modulus of elasticity and the density, between the modulus and the hardness, between the hardness and the strength, in agreement with the results of our calculations. The differences in the values of structural parameters between our measurements and the published ones seem to be logical. In the case of reaction sintering, the decrease of modulus of elasticity, toughness and strength with increasing porosity was weaker than suggested, because in this material intergranular contacts existed even at densities lower than the possible smallest value of a packing of spheres.

7. Conclusion

The modulus of elasticity, hardness, fracture toughness and strength can be calculated by modelling the structure by a random arrangement of spheres. If this model is valid, the modulus of elasticity, hardness and fracture toughness are quasi-linear functions of the density, consequently a linear relationship exists between them. The strength is a linear function of the other three mechanical properties if the size of the critical defect does not change. The following material-dependent parameters were used in the calculations: the density and the modulus of elasticity of the

fully densified material, the particle size of the starting powder, the theoretical strength necessary for fracture of an intergranular contact, and the size of a critical defect. The assumption used is probably valid in the 0.6–0.9 TD range.

Our measurements on partially sintered silicon nitride-based ceramics gave linear relationships between the modulus of elasticity, the hardness, the four- and three-point bend strengths and the density. Although no fitting parameter has been used, the observed modulus of elasticity–density curve was in good agreement with the calculated one.

It is thought that the results of calculations are valid for materials other than silicon nitride-based ceramic if their grain structure is similar.

Acknowledgement

The authors thank the OTKA Fund for financial support (project 1215). The technical assistance of É. Hajdú, J. Zsoldos and M. Mészáros is greatly acknowledged.

References

1. R. L. COBLE, *J. Appl. Phys.* **32** (1961) 787.
2. N. J. SHAW, *Powder Met. Int.* **21** (1989) 16.
3. H. F. FISCHMEISTER and E. ARZT, *Powder Metall.* **26** (1983) 82.
4. L. CORONEL, J. P. JERNOT and F. OSTERSTOCK, *J. Mater. Sci.* **25** (1990) 4866.
5. G. ZIEGLER, J. HEINRICH and G. WÖTTING, *ibid.* **22** (1987) 3041.
6. G. C. KUCZYNSKI, *Trans. AIME* **185** (1949) 169.
7. R. L. COBLE, *J. Am. Ceram. Soc.* **41** (1958) 55.
8. W. D. KINGERY and M. BERG, *J. Appl. Phys.* **26** (1955) 1205.
9. G. W. SCHERER, *J. Am. Ceram. Soc.* **74** (1991) 1523.
10. O. YEHESKEL, Y. GEFEN and M. TALIANKER, in "Proceedings of the 3rd International Conference on Isostatic Pressing", London, 1986 (Metal Powder Report Publishing Ltd., London, 1986) paper 20-1.
11. A. A. LAYYOUS, P. GREIL and G. PETZOW, in "Proceedings of the 12th Plansee Seminar", Reutte, 1989, edited by H. Bildstein and H. M. Ortner (Metallwerk Plansee, Reutte, 1989) p. 637.
12. M. MITOMO and S. UENOSONO, *J. Am. Ceram. Soc.* **75** (1992) 103.
13. T. EKSTRÖM and M. NYGREN, *ibid.* **75** (1992) 259.
14. O. YEHESKEL and Y. GEFEN, *Mater. Sci. Eng.* **71** (1985) 95.
15. D. J. GODFREY, *Mater. Sci. Technol.* **1** (1985) 510.
16. J. HEINRICH, D. MUNZ and G. ZIEGLER, *Powder Metall. Int.* **14** (1982) 153.
17. R. W. RICE, K. R. McKINNEY, C. CM. WU, S. W. FREIMAN and W. J. M. DONOUGH, *J. Mater. Sci.* **20** (1985) 1392.
18. S. K. DATTA, A. K. MUKHOPADHYAY and D. CHAKRABORTY, *Am. Ceram. Soc. Bull.* **68** (1989) 2098.
19. A. G. EVANS, *J. Am. Ceram. Soc.* **73** (1990) 187.
20. W. A. KAYSSER, in "Proceedings of the 2nd International Conference on Hot Isostastic Pressing – Theories and Applications", Gaithersburg, MD, 1989, edited by R. J. Schaefer and M. Linzer (ASM International, Metals Park, 1991) p. 1.
21. C. D. TURNER and M. F. ASHBY, in "Proceedings of the International Conference on Hot Isostatic Pressing '93", Antwerp, 1993, edited by L. DeLaey, H. Tas, W. Kaysser (Elsevier, Amsterdam, London, 1994) p. 3.
22. J. C. WANG, *J. Mater. Sci.* **19** (1984) 801.
23. C. P. GAZZARA and D. R. MESSIER, *Am. Ceram. Soc. Bull.* **56** (1977) 777.
24. A. KELE, P. ARATÓ, E. BESENYEI, J. LÁBÁR and F. WÉBER, in "Hot Isostatic Pressing – Theory and Applications", Proceedings of the 3rd International Conference, Osaka, 1991, edited by M. Koizumi (Elsevier, London, New York, 1992) p. 85.
25. P. ARATÓ, L. BARTHA, A. KÜHNE and F. THÜMMLER, *Ber. Dtsch. Keram. Ges.* **69** (1992) 383.
26. O. N. GRIGOR'EV, G. N. SAVRANSKAYA, P. ARATÓ and E. BESENYEI, unpublished (1991).
27. P. F. BECHER, *J. Am. Ceram. Soc.* **74** (1991) 255.
28. K. HAYASHI and M. KOSAKAI, in "Proceedings of 12th Plansee Seminar", Reutte, 1989, edited by H. Bildstein and H. M. Ortner (Metallwerk Plansee, Reutte, 1989) p. 747.

Received 29 July 1993
and accepted 20 September 1994